



Blocked radiative heat transport in the hot pyrolytic lower mantle

Sergey S. Lobanov^{a,b,c,*}, Nicholas Holtgrewe^{a,d}, Gen Ito^{b,e}, James Badro^f, Helene Piet^g, Farhang Nabiei^{g,h}, Jung-Fu Linⁱ, Lkhamsuren Bayarjargal^j, Richard Wirth^c, Anja Schreiber^c, Alexander F. Goncharov^{a,k}

^a Geophysical Laboratory, Carnegie Institution of Washington, Washington, DC 20015, USA

^b Department of Geosciences, Stony Brook University, Stony Brook, NY 11794, USA

^c GFZ German Research Centre for Geosciences, Telegrafenberg, 14473 Potsdam, Germany

^d Center for Advanced Radiation Sources, University of Chicago, IL 60637, USA

^e CNRS Centre de Recherches Pétrographiques et Géochimiques, 54500 Vandoeuvre, France

^f Institut de physique du globe de Paris, Université de Paris, CNRS, 75005 Paris, France

^g Earth and Planetary Science Laboratory, Ecole Polytechnique Fédérale de Lausanne, CH-1015 Lausanne, Switzerland

^h Centre Interdisciplinaire de Microscopie Electronique, Ecole Polytechnique Fédérale de Lausanne, CH-1015 Lausanne, Switzerland

ⁱ Department of Geological Sciences, Jackson School of Geosciences, The University of Texas at Austin, Austin, TX 78712, USA

^j Institute of Geosciences, Goethe University Frankfurt am Main, Frankfurt am Main, Germany

^k Key Laboratory of Materials Physics, Institute of Solid State Physics, CAS, Hefei 230031, China

ARTICLE INFO

Article history:

Received 12 November 2019

Received in revised form 19 February 2020

Accepted 20 February 2020

Available online xxx

Editor: J. Brodholt

Keywords:

thermal conductivity

high pressure

time-resolved spectroscopy

core-mantle boundary

diamond anvil cell

ABSTRACT

The heat flux across the core-mantle boundary (Q_{CMB}) is the key parameter to understand the Earth's thermal history and evolution. Mineralogical constraints of the Q_{CMB} require deciphering contributions of the lattice and radiative components to the thermal conductivity at high pressure and temperature in lower mantle phases with depth-dependent composition. Here we determine the radiative conductivity (k_{rad}) of a realistic lower mantle (pyrolyte) *in situ* using an ultra-bright light probe and fast time-resolved spectroscopic techniques in laser-heated diamond anvil cells. We find that the mantle opacity increases critically upon heating to ~ 3000 K at 40–135 GPa, resulting in an unexpectedly low radiative conductivity decreasing with depth from ~ 0.8 W/m/K at 1000 km to ~ 0.35 W/m/K at the CMB, the latter being ~ 30 times smaller than the estimated lattice thermal conductivity at such conditions. Thus, radiative heat transport is blocked due to an increased optical absorption in the hot lower mantle resulting in a moderate CMB heat flow of ~ 8.5 TW, on the lower end of previous Q_{CMB} estimates based on the mantle and core dynamics. This moderate rate of core cooling implies an inner core age of about 1 Gy and is compatible with both thermally- and compositionally-driven ancient geodynamo.

© 2020 Elsevier B.V. All rights reserved.

1. Introduction

Heat exchange rate between the mantle and core (Q_{CMB}) is of primary importance for mantle convection and core geodynamo, the two processes that have been paramount for life on Earth. Considerations of the mantle and core energy budgets suggest a Q_{CMB} in the range of 10–16 TW (e.g. Nimmo, 2015). Independently, transport properties of the mantle can provide insights into the Q_{CMB} as it is controlled by the thermal conductivity of the mantle rock at the core-mantle boundary (CMB). Total thermal conductivity of primary lower mantle minerals is a sum of its lattice

and radiative components ($k_{total} = k_{lat} + k_{rad}$). At near-ambient temperatures ($T \sim 300$ K) the dominant mechanism of heat conduction is lattice vibrations while radiative transport is minor. At high temperature, however, the radiative mechanism is expected to become much more effective (Clark, 1957) as $k_{rad}(P, T) \sim \frac{T^3}{\alpha(P, T)}$ (Eq. 1), where $\alpha(P, T)$ is the pressure- and temperature-dependent light absorption coefficient of the conducting medium. Mantle k_{rad} is expected to increase with depth and light radiation might even be the dominant mechanism of heat transport in the hot thermal boundary layer (TBL) a few hundred km above the core (Hofmeister, 2014; Keppler et al., 2008). To reconstruct mantle radiative thermal conductivity one needs to know the absorption coefficient of representative minerals in the near-infrared (IR) and visible (VIS) range collected at P - T along the geotherm.

Light diffusion in the hot lower mantle is governed by absorption mechanisms in iron-bearing bridgmanite (Bgm), post-

* Corresponding author at: GFZ German Research Centre for Geosciences, Telegrafenberg, 14473 Potsdam, Germany.

E-mail address: slobanov@gfz-potsdam.de (S.S. Lobanov).

perovskite (Ppv), and ferropericlasite (Fp) as these minerals have absorption bands in the near-infrared (IR) and visible (VIS) range (Goncharov et al., 2009, 2008, 2015; Keppler et al., 2008). The intensity and position of absorption bands in the spectra of iron-bearing minerals vary with pressure (Goncharov et al., 2009, 2008, 2015; Keppler et al., 2008) and temperature (Thomas et al., 2012; Ullrich et al., 2002). For example, previous room-temperature studies identified an increase in the absorption coefficient of Fp up to 135 GPa associated primarily with the spin transition and red-shift of the Fe-O charge transfer band (Goncharov et al., 2006; Keppler et al., 2007). Likewise, studies of upper mantle minerals at moderate temperatures have recognized substantial variations in their absorption spectra in the IR-VIS range. Crystal field and Fe-O charge transfer bands in olivine show an apparent intensification and broadening upon heating to 1700 K at 1 atm (Ullrich et al., 2002). Similarly, characteristics of the Fe^{2+} - Fe^{3+} charge transfer bands in wadsleyite and ringwoodite are altered upon heating to ~ 800 K (Thomas et al., 2012). Although these transformations cannot be reliably extrapolated to temperatures of several thousand Kelvin, these absorption mechanisms govern the optical properties of Bgm, Fp, and Ppv in the lower mantle, and thus must affect their radiative conductivity. Despite the importance, optical properties of Bgm, Ppv, and Fp have never been measured at mantle P - T conditions as such measurements are challenging because of the thermal radiation interfering with the probe light at high T . On top of the P - and T -dependence of optical properties, absorption coefficients are sensitive to iron concentration, its valence/spin state, and crystallographic environment. In the mantle all of these vary with depth in a complex and not yet fully understood way (Irifune et al., 2010), contributing to the uncertainty in the mantle k_{rad} . As a result of these complications, current k_{rad} models are exclusively based on room-temperature measurements of Bgm and Fp with fixed chemical composition (Goncharov et al., 2009, 2008, 2015; Keppler et al., 2008).

2. Experimental methods

Optical measurements at high P - T were performed in laser-heated diamond anvil cells (DACs) using an ultra-bright light probe synchronized with fast time-resolved IR and VIS detectors (Lobanov et al., 2016, 2017) that allowed us to diminish the contribution of thermal background (more details are provided in Supplementary Materials). We determine the radiative conductivity of the lower mantle by measuring the spectral optical depth in pyrolite, a chemical proxy of the mantle (Irifune et al., 2010), along the Earth's geotherm. Samples of highly homogeneous pyrolite glass (Supplementary Table S1) were crystallized at the thermodynamic conditions of the lower mantle producing a conglomerate of Bgm (\pm Ppv) and Fp with compositions representative of the equilibrium in the lower mantle (Fig. 1). The latter allowed us to account for the effects of P - and T -dependent crystal chemistry such as the iron content and its valence/spin states in the lower mantle phases.

Prior to optical measurements, each glass sample was crystallized at $P > 30$ GPa and T up to 3000 K for several minutes. Near-complete glass crystallization ($>80\%$ along the heating laser beam) was confirmed by the disappearance of a diffuse low frequency Raman peak (Boson peak), which is characteristic of glasses (Supplementary Fig. S1). The mineralogical content of all crystallized samples is dominated by Bgm (+Ppv at ~ 134 GPa) and Fp as revealed by the synchrotron x-ray diffraction (XRD) (Supplementary Fig. S2). In addition to XRD characterization, one of the recovered pyrolite samples (~ 2800 K and 56 GPa) was further analyzed using scanning transmission electron microscopy (STEM) and energy-dispersive x-ray spectroscopy (EDX) in order to reveal its fine texture and the chemical composition of constituting minerals (see details on analytical techniques in Supplementary Materials). High-

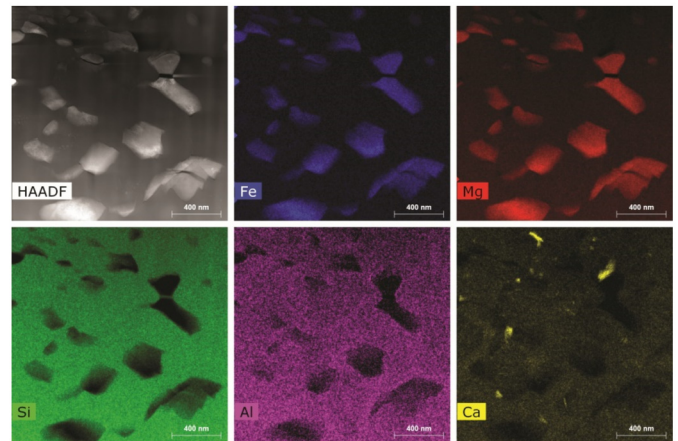


Fig. 1. STEM HAADF image and elemental EDX maps of a pyrolite sample laser-heated at 56 GPa up to ~ 2800 K (see also Supplementary Fig. S3 for the optical image of this sample). Ferropericlasite grains (Si, Al-free) are embedded in the Fe, Al-bearing bridgmanite matrix (Si-rich areas). Ca-perovskite is also present. The scale bar is 400 nm.

angle annular dark-field (HAADF) images show that the grain size of ferropericlasite in the crystallized pyrolite is comparable to the visible light wavelengths (Fig. 1), suggesting that light scattering on grain boundaries might be substantial (Hulst, 1957) and needs to be taken into account. The bulk of the crystallized sample is composed of Bgm, Fp, and Ca-perovskite in the proportions that are consistent with the previous reports on pyrolite mineralogy (~ 75 , 18, and 7 vol.%, respectively, Irifune et al., 2010). Coexisting Bgm and Fp are homogeneous in their chemical composition and show no significant variations across the probed areas with $\text{Bgm}^{\text{Fe}\#} = 7.7 \pm \sim 2$ and $\text{Fp}^{\text{Fe}\#} = 16.8 \pm \sim 2$ (Supplementary Table S2), also in agreement with that reported in the literature (e.g. Irifune et al., 2010). In addition to Bgm, Fp, and Ca-perovskite, we have also observed scarce grains of metallic Fe ($< \sim 1$ vol.%), supporting the notion that the lower mantle may contain a small amount of metallic iron-rich alloy.

3. Results and discussion

Upon heating, our IR-VIS measurements reveal that the optical absorbance of pyrolite shows a continuous strong increase up to the maximum temperature of ~ 2855 K at all studied pressures (Supplementary Fig. S4 and S5). Importantly, the observed temperature-enhanced absorbance is reversible, as is indicated by the similarity of light extinction coefficients (absorption + scattering) measured prior and after the laser-heating cycles, suggesting that the increased opacity at high T is due to a temperature-activated absorption mechanism in the IR-VIS range. Fig. 2 shows pyrolite extinction coefficient at selected P - T conditions that approximate the Earth's geotherm with the exception of the spectrum measured at 134 GPa and 2780 K. The opacity of pyrolite increases by a factor of 4-8 (depending on the frequency) from 40 GPa/2120 K to 134 GPa/2780 K. An even stronger opacity might be expected for the CMB temperatures of ~ 4000 K. Accordingly, we extrapolated the 134 GPa extinction coefficient to 4000 K using its near-linear temperature dependence established in the 1700-2700 K range (Supplementary Materials Fig. S6).

The radiative conductivity of an absorbing medium is given by Clark (1957): $k_{rad}(T) = \frac{4n^2}{3} \int_0^\infty \frac{1}{\alpha(\nu)} \frac{\partial I(\nu, T)}{\partial T} d\nu$ (Eq. 2), where $\alpha(\nu)$ is the frequency-dependent absorption coefficient of the medium, n its refractive index, and $I(\nu, T)$ is the Planck function. Recently, Grose and Afonso (2019) verified the applicability of this equation to evaluating mantle radiative thermal conductivity using numerical modeling. Prior to k_{rad} evaluation, the measured extinction

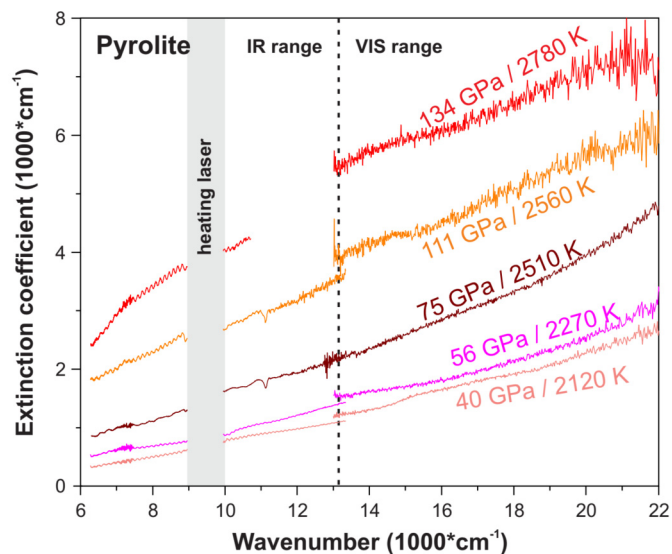


Fig. 2. Pyrolite extinction coefficient at high P - T (before scattering correction). Vertical dashed line divides the IR and VIS ranges as these were measured separately. The 9000–10000 cm^{-1} region is blocked because of the need to filter out the 1070 nm heating laser radiation from reaching the detector. The 11000–13000 cm^{-1} region in the 134 GPa/2710 K spectrum (red) is not shown because of the poor signal-to-background ratio of the IR signal in this range at high absorbance levels.

coefficients were corrected for light scattering in a submicron-grained sample based on the room-temperature absorption coefficients of single crystalline Bgm and Fp with corresponding compositions, which were measured separately using a different optical setup with a conventional (non-laser) optical probe (Goncharov et al., 2009) (Supplementary Materials Fig. S7). Scattering-corrected absorption coefficients measured at P - T conditions approximating the geotherm yield k_{rad} values that decrease continuously with depth from ~ 0.8 W/m/K at 1000 km to ~ 0.1 W/m/K at the top of the TBL (at ~ 2500 km) and then increases to ~ 0.35 W/m/K at the CMB (Fig. 3). Even smaller k_{rad} values may be expected for the lower mantle if its grain size is smaller than the optical depth of pyrolite (< 100 μm) due to light scattering on grain boundaries. However, the grain size of the mantle is likely larger than the photon mean free path because of the hot regime favoring grain growth (e.g. Keppler et al., 2008). The apparent negative slope of radiative thermal conductivity with depth is at odds with all previous radiative conductivity models, which show a positive trend and k_{rad} up to 4–5 W/m/K at the CMB (Goncharov et al., 2015; Hofmeister, 2014; Keppler et al., 2008). These previous models, however, were based on room-temperature measurements (Goncharov et al., 2008, 2015; Keppler et al., 2008) or empirical considerations on the transparency of silicates at high temperature that assumed negligible temperature effect on the mantle optical properties (Hofmeister, 2014). Here we showed that pyrolite optical properties are highly sensitive to T (Supplementary Materials Fig. S4 and S5), suggesting that temperature-enhanced opacity leads to the negative k_{rad} slope with depth.

It is important to address possible sources of uncertainties that may have affected the present estimate of the pyrolite radiative thermal conductivity. First and foremost, systematic errors associated with our correction for light scattering on grain boundaries (Supplementary Materials) may be large. We assess scattering by subtracting the weighted absorption coefficients of Bgm and Fp single crystals (measured independently at similar pressures) from the total measured light extinction signal. Our model of light absorption in finely-grained (100–600 nm) pyrolite is adequate because bulk-like optical properties (e.g. band gap) are characteristic of materials with a grain size of > 10 nm (Segets et al., 2009). In

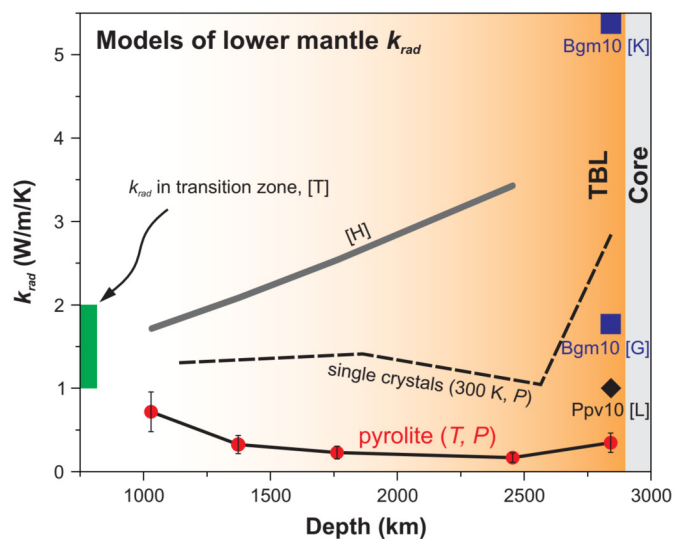


Fig. 3. Radiative conductivity of the pyrolitic lower mantle along the geotherm (Stacey and Davis, 2008) (red circles). The absorption coefficient for 2850 km was projected to 4000 K assuming a linear temperature-dependence of absorbance at $T > 2780$ K (Supplementary Fig. S6). The error bars reflect propagated uncertainties in the refractive index and sample thickness (Supplementary Materials). Black dashed line is the radiative conductivity model based on room-temperature absorption coefficients of single crystalline Bgm and Fp (Supplementary Fig. S7) weighted by their expected fractions in the pyrolitic lower mantle model (0.8 and 0.2, respectively). This model estimates the upper limit on radiative conductivity as it is based on data for single crystals with smaller iron content than expected in pyrolite and does not account for the strong temperature-dependence of absorption spectra revealed in this work. Grey thick curve marked [H] is the thermodynamic model of Hofmeister (2014): $k_{\text{rad}} = 1.9 \times 10^{-10} \times T^3$. Dark blue squares are k_{rad} of Bgm with 10 mol.% Fe based on its 300 K absorption coefficient reported by Keppler et al. (2008) and Goncharov et al. (2015), marked [K] and [G]. Black diamond [L] is k_{rad} of Ppv with 10 mol.% Fe (Lobanov et al., 2017). Green bar [T] is the range of k_{rad} values expected in the transition zone (Thomas et al., 2012). TBL is for thermal boundary layer above the core-mantle boundary. The color gradation illustrates the distribution of temperature in the lower mantle. (For interpretation of the colors in the figure(s), the reader is referred to the web version of this article.)

this approach, however, we used single crystals with lower iron content (6 and 13 mol.% Fe in Bgm and Fp, respectively) than measured in our pyrolite (8 and 18 mol.% Fe) (Supplementary Table S2). As a result, scattering is overestimated and the absorption coefficient of pyrolite is underestimated, which, in turn, results in an overestimation of k_{rad} . The distribution and grain size of relatively transparent Bgm and highly opaque Fp within the synthesized sample may also bear on the measured absorptivity. However, the submicron-sized grains of Fp show a relatively homogeneous distribution in the Bgm matrix (Fig. 1) which, together with the relatively large sample thickness (> 6 μm), ensure that both Bgm and Fp are probed in proportions representative of pyrolite. We also estimated an upper bound on the radiative conductivity using the absorption coefficients of single crystalline Bgm (6 mol.% Fe) and Fp (13 mol.% Fe) mixed in the expected proportions of 0.8 and 0.2 (dashed line in Fig. 3). This model is effectively a Hashin-Shtrikman average of individual radiative conductivities of these single crystalline Bgm and Fp and it likely overestimates k_{rad} because (i) it does not account for the strong temperature-enhanced absorptivity revealed in this work and (ii) it is based on phases with smaller iron content than in pyrolite. In addition to the potential sources of error discussed above, we propagate the errors associated with the ambiguities in the refractive index (uncertain within $\pm 10\%$) and sample thickness ($\pm 20\%$), both intervals being very conservative (see Supplementary Material for discussion), which together contribute an uncertainty of approximately 30% to the estimated k_{rad} and are the basis for the error bars in Fig. 3.

Light absorption in pyrolite at high P - T is governed by specific absorption mechanisms in its constituent phases. In order to disentangle the contribution of Bgm and Fp to the high-temperature spectra of pyrolite we measured the absorption coefficient of Bgm (single crystal, 6 mol.% Fe) up to ~ 2500 K (Supplementary Fig. S8). Surprisingly, the absorption coefficient of Bgm increases with the rate of $\sim 0.1 \text{ cm}^{-1}/\text{K}$, while a much stronger temperature-dependence of $\sim 0.4 \text{ cm}^{-1}/\text{K}$ is characteristic of pyrolite (Supplementary Fig. S6). This observation hints that the strong increase in pyrolite absorbance at high temperature is not due to Bgm but is a result of the temperature-enhanced opacity of Fp. Unfortunately, we could not obtain reliable high-temperature absorption spectra of Fp as it showed irreversible changes in absorbance over continuous laser heating at $T > 1000$ K. We tentatively attribute this behavior to Soret-like iron diffusion under the steep temperature gradient typical of laser-heated samples. Cation diffusion rates in Fp are ~ 2 orders of magnitude faster than in Bgm (Ammann et al., 2010), which may be why reversible spectroscopic behavior is preserved in Bgm upon continuous laser heating up to $T > 2500$ K. In the pyrolite sample iron diffusion is further limited by the small grain size and the reversible spectroscopic behavior is preserved below ~ 3000 K (at 134 GPa). We note that while we cannot rule out significant Soret-like iron diffusion in the crystallized pyrolite, it would tend to lower the measured light absorption coefficient because of the iron migration out of the probed spot and, accordingly, would increase the inferred k_{rad} . Therefore, the reported very low values of radiative conductivity are not caused by Soret-like diffusion.

To suppress iron diffusion and directly compare the temperature-induced changes in the Bgm and Fp optical absorbance we decreased the total laser-heating time by a factor of $\sim 10^6$ in an independent series of dynamically-heated DAC experiments. Fully reversible optical absorbance was observed in Bgm and Fp over the single-shot $1 \mu\text{s}$ long laser-heating to $T > 3000$ K at 111–135 GPa (Supplementary Fig. S9). Upon heating to ~ 3000 K at 135 GPa, Fp becomes ~ 5 times opaquer than it is at room temperature. In contrast, Bgm is only 20–30% opaquer at ~ 3500 K than at room temperature. Because these transformations are fully reversible, they must reflect temperature-induced changes in light absorption by these single crystals. Our new streak camera data unambiguously show that light absorption in Fp is much more sensitive to temperature than in Bgm, confirming that the optical opacity of the lowermost mantle, and by extension its radiative conductivity, is governed by Fp. Such a diverse high-temperature behavior of Fp and Bgm likely results from the different mechanisms that govern light extinction in these phases. Even at room temperature single crystalline Fp with 13 mol.% Fe at 117 GPa is 2–3 times opaquer than Bgm with 6 mol.% Fe due to the intense Fe-O charge transfer band that extends into the VIS range. Lattice vibrations in hot Fp dynamically decrease the Fe-O separation, red-shifting the Fe-O charge transfer band, narrowing the band gap, and serving as a physical mechanism that effectively blocks radiative heat transport in the lowermost mantle. The proposed mechanism is much less effective in Bgm which accommodates iron predominantly at the larger (dodecahedral) site with longer average Fe-O distances than in Fp.

The high-pressure high-temperature behavior of Fp is of key importance for a pyrolytic model, indicating that Fp plays a major role in the opacity of the lower mantle and the effectiveness of radiative heat transport. In addition, the decreased band gap enhances electrical conductivity of Fp in the narrow depth range of the TBL (< 100 km) where the temperature increase is sharpest. Our interpretation of the optical behavior of Fp at high P - T is in qualitative agreement with the computational evidence for a very high electrical conductivity ($\sim 4 \cdot 10^4 \text{ S/m}$) in Fp at CMB conditions due to iron d -states forming broad bands near the Fermi level

(Holmstrom and Stixrude, 2015). As such, our work hints that the physical properties of Fp contribute complexity to the CMB region and are responsible for some of its exotic features. For example, temperature-enhanced electrical conductivity of Fp in the TBL can account for the apparent absence of lag between the fluctuation in day length and geomagnetic jerks, which requires a thin (< 50 km) layer of highly conducting mantle just above the core (Holme and de Viron, 2013).

Firmly constrained total thermal conductivity at the base of the mantle offers valuable insights into the CMB heat flow through the Fourier law of heat conduction: $Q_{CMB} = A_{CMB} * k_{total} * \Delta T$, where A_{CMB} is the surface area of the CMB and ΔT is the temperature gradient above the CMB. Experimental estimates of the lattice thermal conductivity for a 4:1 mixture of Bgm (or Ppv) and Fp at CMB conditions fall in the range of 7.7–8.8 W/m/K (Supplementary Table S3) (Dalton et al., 2013; Ohta et al., 2017; Okuda et al., 2017). While these values are based on measurements in DACs at 300 K and rely on extrapolations to CMB temperatures, they are consistent with *ab initio* calculations of lower mantle thermal conductivity (Stackhouse et al., 2015) as well as a recent experimental study of the lattice conductivity in Fe- and Fe,Al-bearing Bgm (Hsieh et al., 2017). Recent estimates of the total thermal conductivity at the base of the mantle accepted k_{rad} of ~ 2 –4 W/m/K (e.g. Ohta et al., 2017; Okuda et al., 2017). The results of this work clearly indicate that radiative conductivity is not an important mechanism of heat transport in the lowermost mantle and may be safely neglected from estimates of the total thermal conductivity at the CMB. Accepting $k_{total} \approx k_{lat} \approx 8.5 \text{ W/m/K}$ and a temperature gradient of $\sim 0.007 \text{ K/m}$ in the TBL (Stacey and Davis, 2008), we obtain a Q_{CMB} of $\sim 8.5 \text{ TW}$ for the present-day CMB.

This rate of heat extraction out of the core is sufficient to drive the present-day geodynamo, thanks to the compositional buoyancy due to the inner core growth, and is consistent with the inner core young age of ~ 0.6 –1.3 Gy (e.g. Labrosse et al., 2001), assuming radioactive heat production is small in the core. A much older Earth's magnetic record (Hadean-Paleoarchean) requires a geodynamo prior to the inner core nucleation, operating in a convecting liquid core. Two distinct scenarios follow from the low mantle thermal conductivity. If core thermal conductivity is relatively low ($< 50 \text{ W/m/K}$) (Konopkova et al., 2016; Stacey and Loper, 2007), a CMB heat flux that is greater than the core adiabatic heat flux enables a thermally-driven geodynamo in the ancient fully molten core (Nimmo, 2015). Alternatively, high core thermal conductivity ($> 100 \text{ W/m/K}$) (Ohta et al., 2016; Pozzo et al., 2012) is inconsistent with a thermally-driven geodynamo, and requires a compositionally-driven convection powered by light element exsolution upon core cooling (Badro et al., 2016; Hirose et al., 2017; O'Rourke and Stevenson, 2016). Even if an early geodynamo can be driven in the cooling ancient molten core, determining its exact driving mechanism requires a definitive assessment of Earth's core thermal conductivity. Beyond Earth's magnetic field, our results shed light on the plausibility of long-lived dynamos in other terrestrial planets and exoplanets, and could provide a discriminating argument for their past or present habitability.

Acknowledgements

SSL acknowledges the support of the Helmholtz Young Investigators Group CLEAR (VH-NG-1325). JB acknowledges support from IGP multidisciplinary program PARI, and by Paris-IdF region SESAME Grant no. 12015908 and UnivEarthS Labex program at Sorbonne Paris Cité (ANR-10-LABX-0023 and ANR-11-IDEX-0005-02). This work was supported by the NSF Major Research Instrumentation program DMR-1039807, NSF EAR-1520648 and NSF EAR-1763287, NSF EAR/IF-1128867, the Army Research Office (56122-CH-H and 71650-CH), the Carnegie Institution of Washington and

Deep Carbon Observatory. The authors acknowledge T. Okuchi and N. Purevjav for their assist with the synthesis of the bridgmanite sample at Okayama University at Misasa. JFL acknowledges support from Geophysics Program of the National Science Foundation of the United States (EAR-1916941). Parts of this work were conducted at GSECARS 13IDD beamline of the Advanced Photon Source, Argonne National Laboratory. GeoSoilEnviroCARS (Sector 13), Advanced Photon Source (APS), Argonne National Laboratory is supported by the National Science Foundation – Earth Sciences (EAR-1128799) and Department of Energy – GeoSciences (DE-FG02-94ER14466). This research used resources of the Advanced Photon Source, a U.S. Department of Energy (DOE) Office of Science User Facility operated for the DOE Office of Science by Argonne National Laboratory under Contract No. DE-AC02-06CH11357.

Declaration of competing interest

The authors declare no conflict of interest.

Appendix A. Supplementary material

Supplementary material related to this article can be found online at <https://doi.org/10.1016/j.epsl.2020.116176>.

References

- Ammann, M.W., Brodholt, J.P., Wookey, J., Dobson, D.P., 2010. First-principles constraints on diffusion in lower-mantle minerals and a weak D'' layer. *Nature* 465, 462–465.
- Badro, J., Siebert, J., Nimmo, F., 2016. An early geodynamo driven by exsolution of mantle components from Earth's core. *Nature* 536, 326–328.
- Clark, S.P., 1957. Radiative transfer in the Earth's mantle. *Eos Trans. AGU* 38, 931–938.
- Dalton, D.A., Hsieh, W.P., Hohensee, G.T., Cahill, D.G., Goncharov, A.F., 2013. Effect of mass disorder on the lattice thermal conductivity of MgO periclase under pressure. *Sci. Rep.* 3, 02400.
- Goncharov, A.F., Beck, P., Struzhkin, V.V., Haugen, B.D., Jacobsen, S.D., 2009. Thermal conductivity of lower-mantle minerals. *Phys. Earth Planet. Inter.* 174, 24–32.
- Goncharov, A.F., Haugen, B.D., Struzhkin, V.V., Beck, P., Jacobsen, S.D., 2008. Radiative conductivity in the Earth's lower mantle. *Nature* 456, 231–234.
- Goncharov, A.F., Lobanov, S.S., Tan, X., Hohensee, G.T., Cahill, D.G., Lin, J.F., Thomas, S.M., Okuchi, T., Tomioka, N., 2015. Experimental study of thermal conductivity at high pressures: implications for the deep Earth's interior. *Phys. Earth Planet. Inter.* 247, 11–16.
- Goncharov, A.F., Struzhkin, V.V., Jacobsen, S.D., 2006. Reduced radiative conductivity of low-spin (Mg,Fe)O in the lower mantle. *Science* 312, 1205–1208.
- Grose, C.J., Afonso, J.C., 2019. New constraints on the thermal conductivity of the upper mantle from numerical models of radiation transport. *Geochem. Geophys. Geosyst.* 20, 2378–2394.
- Hirose, K., Morard, G., Sinmyo, R., Umemoto, K., Hernlund, J., Helffrich, G., Labrosse, S., 2017. Crystallization of silicon dioxide and compositional evolution of the Earth's core. *Nature* 543, 99–102.
- Hofmeister, A.M., 2014. Thermodynamic and optical thickness corrections to diffusive radiative transfer formulations with application to planetary interiors. *Geophys. Res. Lett.* 41, 3074–3080.
- Holme, R., de Viron, O., 2013. Characterization and implications of intradecadal variations in length of day. *Nature* 499, 202–204.
- Holmstrom, E., Stixrude, L., 2015. Spin crossover in ferropericlase from first-principles molecular dynamics. *Phys. Rev. Lett.* 114, 117202.
- Hsieh, W.P., Deschamps, F., Okuchi, T., Lin, J.F., 2017. Reduced lattice thermal conductivity of Fe-bearing bridgmanite in Earth's deep mantle. *J. Geophys. Res., Solid Earth* 122, 4900–4917.
- Hulst, H.C.v.d., 1957. *Light Scattering by Small Particles*. Wiley, New York.
- Irifune, T., Shinmei, T., McCammon, C.A., Miyajima, N., Rubie, D.C., Frost, D.J., 2010. Iron partitioning and density changes of pyrolite in Earth's lower mantle. *Science* 327, 193–195.
- Keppler, H., Dubrovinsky, L.S., Narygina, O., Kantor, I., 2008. Optical absorption and radiative thermal conductivity of silicate perovskite to 125 gigapascals. *Science* 322, 1529–1532.
- Keppler, H., Kantor, I., Dubrovinsky, L.S., 2007. Optical absorption spectra of ferropericlase to 84 GPa. *Am. Mineral.* 92, 433–436.
- Konopkova, Z., McWilliams, R.S., Gomez-Perez, N., Goncharov, A.F., 2016. Direct measurement of thermal conductivity in solid iron at planetary core conditions. *Nature* 534, 99–101.
- Labrosse, S., Poirier, J.P., Le Mouel, J.L., 2001. The age of the inner core. *Earth Planet. Sci. Lett.* 190, 111–123.
- Lobanov, S.S., Holtgrewe, N., Goncharov, A.F., 2016. Reduced radiative conductivity of low spin FeO₆-octahedra in FeCO₃ at high pressure and temperature. *Earth Planet. Sci. Lett.* 449, 20–25.
- Lobanov, S.S., Holtgrewe, N., Lin, J.F., Goncharov, A.F., 2017. Radiative conductivity and abundance of post-perovskite in the lowermost mantle. *Earth Planet. Sci. Lett.* 479, 43–49.
- Nimmo, F., 2015. 8.02 - Energetics of the core A2 - Schubert, Gerald. In: Schubert, G. (Ed.), *Treatise on Geophysics*, second edition. Elsevier, Oxford, pp. 27–55.
- O'Rourke, J.G., Stevenson, D.J., 2016. Powering Earth's dynamo with magnesium precipitation from the core. *Nature* 529, 387–389.
- Ohta, K., Kuwayama, Y., Hirose, K., Shimizu, K., Ohishi, Y., 2016. Experimental determination of the electrical resistivity of iron at Earth's core conditions. *Nature* 534, 95–98.
- Ohta, K., Yagi, T., Hirose, K., Ohishi, Y., 2017. Thermal conductivity of ferropericlase in the Earth's lower mantle. *Earth Planet. Sci. Lett.* 465, 29–37.
- Okuda, Y., Ohta, K., Yagi, T., Sinmyo, R., Wakamatsu, T., Hirose, K., Ohishi, Y., 2017. The effect of iron and aluminum incorporation on lattice thermal conductivity of bridgmanite at the Earth's lower mantle. *Earth Planet. Sci. Lett.* 474, 25–31.
- Pozzo, M., Davies, C., Gubbins, D., Alfe, D., 2012. Thermal and electrical conductivity of iron at Earth's core conditions. *Nature* 485, 355–358.
- Segets, D., Gradl, J., Taylor, R.K., Vassilev, V., Peukert, W., 2009. Analysis of optical absorbance spectra for the determination of ZnO nanoparticle size distribution, solubility, and surface energy. *ACS Nano* 3, 1703–1710.
- Stacey, F.D., Davis, P.M., 2008. *Physics of the Earth*, 4th ed. Cambridge University Press, Cambridge, New York.
- Stacey, F.D., Loper, D.E., 2007. A revised estimate of the conductivity of iron alloy at high pressure and implications for the core energy balance. *Phys. Earth Planet. Inter.* 161, 13–18.
- Stackhouse, S., Stixrude, L., Karki, B.B., 2015. First-principles calculations of the lattice thermal conductivity of the lower mantle. *Earth Planet. Sci. Lett.* 427, 11–17.
- Thomas, S.M., Bina, C.R., Jacobsen, S.D., Goncharov, A.F., 2012. Radiative heat transfer in a hydrous mantle transition zone. *Earth Planet. Sci. Lett.* 357, 130–136.
- Ullrich, K., Langer, K., Becker, K.D., 2002. Temperature dependence of the polarized electronic absorption spectra of olivines. Part I - Fayalite. *Phys. Chem. Miner.* 29, 409–419.